Vehicle System Dynamics
Vol. 49, No. 3, March 2011, 433–447

Taylor & Francis
Taylor & Francis Group

Dynamic emulation of road/tyre longitudinal interaction for developing electric vehicle control systems

Chengbin Ma[a]*, Min Xu[b] and Hao Wang[a]

[a]*Electrical and Computer Engineering, University of Michigan–Shanghai Jiaotong University Joint Institute, Shanghai Jiaotong University, 800 Dongchuan Road, Minhang, Shanghai 200240, People's Republic of China;* [b]*Institute of Automotive Engineering, Shanghai Jiaotong University, 800 Dongchuan Road, Shanghai, 200240, People's Republic of China*

(*Received 24 July 2009; final version received 7 December 2009*)

Current research on electric vehicles (EVs) is focusing on the environment and energy aspects. However, electric motors also have much better control performance than conventional internal combustion engines. EVs could not only be 'cleaner' and 'more energy efficient', but also become 'safer' with 'better driving performance'. In this paper, a discrete elasto-plastic friction model is proposed for a dynamic emulation of road/tyre friction in order to validate the control design of EV control systems in laboratory facilities. Experimental results show the dynamic emulation is able to capture the transient behaviour of the road/tyre friction force during braking and acceleration, therefore enabling a more reliable validation of various EV control methods. And the computation of inverse dynamics, which usually needs to be considered in conventional emulation approaches, can be avoided using the proposed dynamic friction model.

Keywords: dynamic emulation; road/tyre friction; electric vehicle; control systems

1. Introduction

It has been widely recognised that electrifying vehicles can provide a solution to the emission and oil shortage problems brought by billions of conventional vehicles today, which are propelled by internal combustion engines. Consequently, most of the current researches on electric vehicles (EVs) (EVs including the hybrid EVs) are focusing on the environment and energy aspects. And one of the key issues to commercialise EVs is considered to rely largely on the development of long-term energy storage devices with competitive cost.

However, one of the most fundamental differences between EVs and the conventional vehicle is that EVs are the vehicles with one or more electric motors for propulsion instead of using the internal combustion engines; namely the motion of EVs is provided either by wheels driven or partly driven by electric motors, i.e. EVs are actually typical mechatronic systems just like hard disks, robots, machine tools, etc. By introducing the well-developed

*Corresponding author. Email: chbma@sjtu.edu.cn

ISSN 0042-3114 print/ISSN 1744-5159 online

DOI: 10.1080/00423110903545172
http://www.informaworld.com

mechatronic technologies, especially the mechatronic control, EVs are not only 'cleaner' and 'more energy efficient', but also become 'safer' with 'better driving performance' compared with the conventional vehicles. Several researches have been done on this aspect of EVs [1]; however, it is still not well recognised by the public.

From the viewpoint of control, the most distinct advantages of well-controlled electric motors over the internal combustion engines and hydraulic braking systems are as follows:

(1) Millisecond-level torque response (10–100 times faster).
(2) Accurate feedback of the generated motor current/torque (motor torque $\propto$ motor current).
(3) Continuously variable speed in nature (see the torque–speed characteristics of electric motors shown in Figure 1).
(4) Small size but powerful output (easy to implement distributed motor location using in-wheel motors).

The above unique advantages of electric motors make it possible to achieve high-performance motion control of EVs with flexible and simplified configurations.

Like the development of other mechatronic systems, model-based emulation is convenient for validating the design of EV control systems such as the anti-skid control and yaw dynamics control systems, especially in laboratory facilities. Test benches have been developed for serving the validation and experimental purposes ranging from the design and test of propulsion motor drives to the implementation of Hardware-In-the-Loop powertrain control strategies [2–5]. The test benches usually have the following three main components: a dynamometer, a real-time data acquisition and digital control system, and a propulsion drive motor under test. However, in those test benches, the conventional dynamometers are normally controlled to deliver a particular steady-state torque–speed relationship, in which no tyre sliding (complete road/tyre adhesion) is assumed. Although useful for evaluating the basic performance of the system, these dynamometers are not satisfactory for examining the transient behaviour during braking and acceleration of the vehicle.

As emphasised above, the high-performance vehicle control of EVs could be achieved by taking full advantage of the electric motor's unique characteristics. Since the friction force at the road/tyre interface is the main mechanism for converting wheel angular acceleration to linear acceleration, i.e. generating longitudinal force, the emulation of friction force characteristics at the road/tyre interface is important for developing and validating EV control

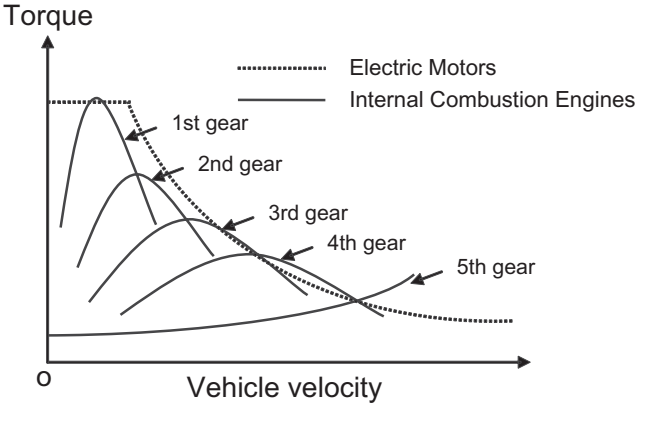

Figure 1. The torque–speed characteristics of electric motors and internal combustion engines.

systems, which rely on the knowledge of the friction characteristics. The friction model for emulating the road/tyre interaction need be able to capture accurately the transient behaviour of the friction force during braking and acceleration.

This paper describes a dynamometer strategy based on a discrete elasto-plastic friction model for a dynamic emulation of the road/tyre interaction, which is expected to be useful for the validation of the design of EV control systems in laboratory facilities. Because compared with the static friction models, the dynamic friction model is able to capture the transient behaviour of the friction force during braking and acceleration. A case study, disturbance observer (DOB)-based anti-skid control of EVs, is introduced in order to test the proposed dynamic emulation experimentally.

2. Laboratory test benches

As shown in Figure 2, basically the test benches have the following three main components: a dynamometer, a real-time data acquisition and digital control system, and a propulsion drive motor under test. The dynamometer and the drive motor are usually vector-controlled AC motors using pulse-width modulation (PWM) inverters. The two motors are on a common shaft, which are controlled using a microprocessor system. A PC can be used as a user interface and data capture facilities for the feedback signals of the motor current and angular speed of motors. The drive motor including its inverter provide the target system for research on EV control strategies. The dynamometer (load motor) is controlled so that the mechanical rig dynamics, which is defined as the speed response to a given drive torque, is equivalent to the mechanical load dynamics of EV's longitudinal motion, i.e. the longitudinal dynamics. In this way, the emulation preserves the physical causality of an EV in which the motion variables are the output responses to a drive torque.

For the control of conventional dynamometers, the equivalent equation to emulate EV's longitudinal dynamics can be written as

$$J_e\dot{\omega} = T_m - T_g - T_a - T_r \tag{1}$$

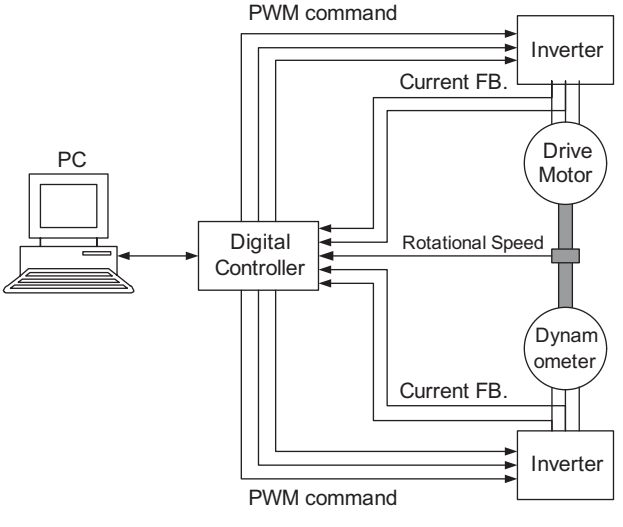

Figure 2. EV test bench.

where J_e is the equivalent inertia of the vehicle, ω is the angular velocity of motor, T_m is the drive torque, T_g, T_a and T_r are the equivalent torques for the slope resistance, aerodynamic drag and rolling resistance, respectively, as shown in the following equations:

$$T_g = Mg \sin\alpha \cdot r \tag{2}$$

$$T_a = \frac{1}{2}\rho A C V^2 \cdot r \tag{3}$$

$$T_r = Mgf_r \cos\alpha \cdot r \tag{4}$$

where M is the vehicle mass, r is the wheel radius, g is the gravity, α is the road slope angle, ρ is the air density, A is the frontal area of the vehicle, C is the aerodynamic drag coefficient and V is the linear velocity of the vehicle.

Under the assumption of no tyre sliding (complete road/tyre adhesion), namely

$$V = r\omega. \tag{5}$$

The equivalent inertia J_e can be calculated as

$$J_e = J_w + Mr^2 \tag{6}$$

where J_w is the wheel inertia. Therefore a straightforward way to calculate the torque of the dynamometer T_d that need to be generated is

$$T_d = Mg \sin\alpha \cdot r + \frac{1}{2}\rho A C (r\omega)^2 \cdot r + Mgf_r \cos\alpha \cdot r + (J_e - J_t) \cdot \dot{\omega} \tag{7}$$

where J_t is the total inertia of the drive motor, dynamometer and the connecting shaft. However, T_d is calculated based on the inverse dynamic of $(J_e - J_t) \cdot \dot{\omega}$, in which the angular velocity ω is measured and used to derive the desired torque of the dynamometer such as using a backward difference approximation

$$\dot{\omega}(k) = \frac{\omega(k) - \omega(k-1)}{T_s} \tag{8}$$

where T_s is the sampling time.

In practice, noise problems prohibit the use of small sampling time for the computation of the inverse dynamics. And the discretisation effects lead to the instability of the system. Inverse dynamics, i.e. the need to compute acceleration, should be avoided. A model speed tracking approach can be applied to avoid the usage of inverse dynamics [6]. As shown in the block diagram of the approach (Figure 3), a controller $G_c(s)$ and a compensation

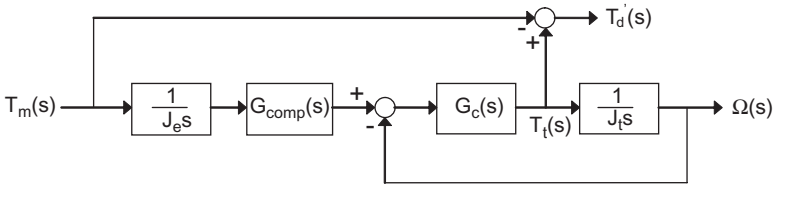

Figure 3. Block diagram of the model speed tracking approach.

term $G_{\text{comp}}(s)$ can be introduced, where

$$G_{\text{comp}}(s) = \frac{1 + G_{\text{c}}(s)\frac{1}{J_{\text{t}}s}}{G_{\text{c}}(s)\frac{1}{J_{\text{t}}s}}. \tag{9}$$

Therefore, the transfer function from the drive torque T_{m} to the angular velocity ω is

$$\frac{\Omega(s)}{T_{\text{m}}(s)} = \frac{1}{J_{\text{e}}s} \cdot G_{\text{comp}}(s) \cdot \frac{G_c(s)\frac{1}{J_{\text{t}}s}}{1 + G_c(s)\frac{1}{J_{\text{t}}s}} = \frac{1}{J_{\text{e}}s}. \tag{10}$$

And the torque of dynamometer T'_{d} that need to be generated for emulating the effect of the equivalent inertia J_{e} can be calculated as

$$T'_{\text{d}} = T_{\text{t}} - T_{\text{m}} \tag{11}$$

where T_{t} is the output of the controller $G_{\text{c}}(s)$.

3. Review of road/tyre friction models

As mentioned above, for the conventional control of the dynamometer, the complete road/tyre adhesion is assumed which totally neglects the main mechanism for the motion of vehicles. In order to capture the transient behaviour of the road/tyre friction, a proper friction model needs to be introduced for computing the torque that needs to be generated by the dynamometer. In this paper, a simplified motion dynamics of a quarter-vehicle model is considered. Unlike in Equation (1), the longitudinal dynamics is of the form:

$$\frac{M}{4}\dot{v} = F \tag{12}$$

$$J_{\text{w}}\dot{\omega} = -rF + T_{\text{m}} \tag{13}$$

where v is the linear velocity of the vehicle and F is the road/tyre friction force. For the sake of simplicity, the slope resistance, aerodynamic drag and rolling resistance are neglected.

For most road/tyre friction models, a common assumption is that the normalised tyre friction μ, which is defined as

$$\mu = \frac{F}{F_n} = \frac{\text{Friction Force}}{\text{Normal Force}} \tag{14}$$

is a nonlinear function of the relative velocity between the road and the tyre with a distinct maximum value.

3.1. *Static slip/friction models*

The static slip/friction models are the most common road/tyre friction models used in the simulation of vehicle longitudinal dynamics. As shown in Figure 4, they are defined as one-to-one maps between the friction F, and the longitudinal slip rate s, which is defined as

$$\begin{cases} s = \dfrac{r\omega}{v} - 1, \text{ if } v > r\omega \text{ and } v \neq 0 \text{ for braking} \\ s = 1 - \dfrac{v}{r\omega}, \text{ if } v < r\omega \text{ and } \omega \neq 0 \text{ for acceleration} \end{cases} \tag{15}$$

where v and ω are the linear and angular velocities, respectively.

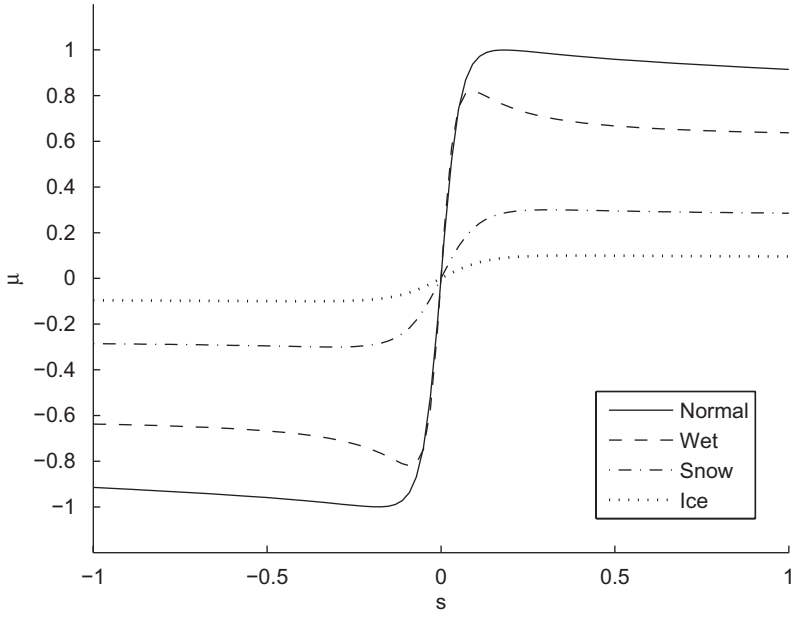

Figure 4. Plot of static slip/friction characteristics.

One of the most well-known static slip/friction models is Pacejka's model, also known as the 'Magic Formula' [7]. This model has been shown to match experimental data suitably, obtained under particular road conditions with various combinations of the constant linear and angular velocities. Pacejka's model has the form

$$F(s) = c_1 \sin(c_2 \arctan(c_3 s - c_4(c_3 s - \arctan(c_3 s)))) \tag{16}$$

where the parameters $c_1, \ldots, c_4$ can be identified by fitting a given set of road/tyre test data.

The static friction models assume the ideal steady-state conditions for the constant linear and angular velocities, i.e. v and ω in Equations (12) and (13). However, in reality, the linear and angular velocities can never be controlled independently. Such ideal steady-state conditions can only be reached during constant speed cruising. The dynamic nature of the road/tyre friction need to be modelled for exhibiting transient behaviour which may differ significantly from its steady-state value.

3.2. *Dynamic friction models*

The dynamic friction models attempt to describe the transient behaviour of the friction force. There are two types of dynamic friction models, lumped friction models and distributed friction models. The lumped friction models assume a point road/tyre contact; while the distributed ones assume a contact patch existing between the road and the tyre [8]. Naturally the distributed friction models are represented by partial differential equations. Only the lumped friction model is discussed in this paper.

A number of dynamic friction models have been proposed such as the Bristle model, Dahl model, etc [9]. Among those models, the LuGre model is the one of the most popular models for the control system design with the existence of friction [10]. The LuGre model is an extension of the Dahl model with the Stribeck effect.

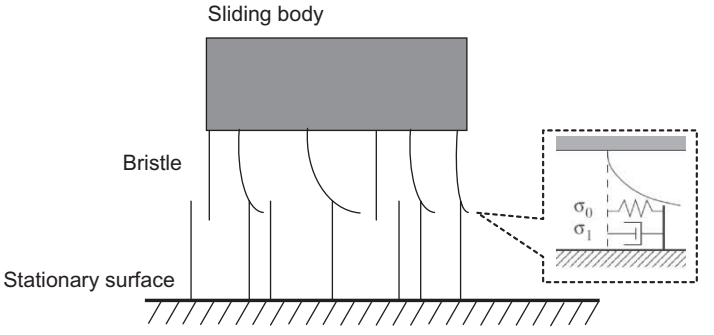

Figure 5. The friction mechanism of the bristle deflection.

In the LuGre model, the mechanism of friction is described by two rigid bodies contacting through elastic bristles, as shown in Figure 5. If the deflection of the bristles is large enough, the bristles will start to slip. An internal state z denotes the average deflection that is modelled by

$$\dot{z} = v_\mathrm{r} - \frac{\sigma_0 |v_\mathrm{r}|}{g(v_\mathrm{r})} z \tag{17}$$

$$g(v_\mathrm{r}) = \mu_\mathrm{c} + (\mu_\mathrm{s} - \mu_\mathrm{c}) \mathrm{e}^{-|v_\mathrm{r}/v_\mathrm{s}|^\eta} \tag{18}$$

where $v_\mathrm{r} = r\omega - v$ is the relative velocity, σ_0 is the stiffness of the bristles, μ_c is the normalised Coulomb friction, μ_s is normalised static friction ($\mu_\mathrm{s} \geq \mu_\mathrm{c}$), v_s is the Stribeck relative velocity, η is introduced to capture the steady-state slip/friction characteristics. Typical value for η is between 0.5 and 2 (η is taken as 0.5 in this paper). Therefore the steady state of z, i.e. when v_r is constant, is

$$z_\mathrm{ss}(v_\mathrm{r}) = \frac{g(v_\mathrm{r})}{\sigma_0 |v_\mathrm{r}|} v_\mathrm{r} = \frac{g(v_\mathrm{r})}{\sigma_0} \mathrm{sgn}(v_\mathrm{r}). \tag{19}$$

The friction force is

$$F = F_\mathrm{n}(\sigma_0 z + \sigma_1 \dot{z} + \sigma_2 v_\mathrm{r}). \tag{20}$$

The first two terms describe the friction force generated from the bending of the bristles, where σ_0 is the stiffness and σ_1 is the damping. The last term is for the viscous force proportional to v_r with coefficient σ_2.

For the level of road/tyre adhesion, it can be modelled by introducing a parameter θ into the function $g(v_\mathrm{r})$:

$$\tilde{g}(v_\mathrm{r}) = \theta g(v_\mathrm{r}). \tag{21}$$

The LuGre model is popular because its parameters have a physical significance and its velocity-dependency is also physically consistent. However, the LuGre model has been known to exhibit spurious unbounded drift subjected to an arbitrarily small external force and arbitrarily small vibrations, which is not a physically consistent behaviour [11]. This non-physical phenomenon results from inaccurate modelling of the presliding as a placement always includes plastic (irreversible) component.

This drawback of the LuGre model can be overcome by having an elsato-plastic presliding, which starts from elastic (reversible) placement, then to mixed elastic and plastic displacement and finally to plastic placement. Assume the rigid body displacement can be decomposed into

elastic and plastic components, z and w, respectively, then the presliding displacement can be categorised using the following equations:

$$\left.\begin{aligned} v_{\mathrm{r}} &= \dot{z} \\ \dot{w} &= 0 \end{aligned}\right\} \text{ elastic displacement} \tag{22}$$

$$v_{\mathrm{r}} = \dot{z} + \dot{w} \text{ mixed elastic and plastic displacement} \tag{23}$$

$$\left.\begin{aligned} v_{\mathrm{r}} &= \dot{w} \\ \dot{z} &= 0 \end{aligned}\right\} \text{ plastic displacement.} \tag{24}$$

In order to describe the elasto-plastic presliding, a piecewise continuous function $\alpha(z, v_{\mathrm{r}})$ can be introduced to control $\dot{z}$:

$$\dot{z} = v_{\mathrm{r}} - \alpha(z, v_{\mathrm{r}}) \frac{\sigma_0 |v_{\mathrm{r}}|}{g(v_{\mathrm{r}})} z \tag{25}$$

where $\alpha(z, v)$ is defined as

$$\alpha(v_{\mathrm{r}}, z) = \begin{cases} 0, & |z| \le z_{\mathrm{ba}},\ \mathrm{sgn}(v_{\mathrm{r}}) = \mathrm{sgn}(z) \\ \alpha_{\mathrm{m}}(v_{\mathrm{r}}, z), & z_{\mathrm{ba}} < |z| < z_{\mathrm{ss}}(v_{\mathrm{r}}), \mathrm{sgn}(v_{\mathrm{r}}) = \mathrm{sgn}(z) \\ 1, & |z| \ge z_{\mathrm{ss}}(v_{\mathrm{r}}), \mathrm{sgn}(v_{\mathrm{r}}) = \mathrm{sgn}(z) \\ 0, & \mathrm{sgn}(v_{\mathrm{r}}) \ne \mathrm{sgn}(z) \end{cases} \tag{26}$$

where z_{ba} is the breakaway displacement below which the presliding is purely elastic. For small displacements $\alpha = 0$ and thus $\dot{z} = v_{\mathrm{r}}$ (purely elastic presliding), while for larger displacements, the mixed elastic–plastic sliding is entered; and finally transitions to purely plastic is achieved with $\alpha = 1$, $\dot{z} = 0$ and $z = z_{\mathrm{ss}}(v_{\mathrm{r}})$ at the steady state.

As shown in Figure 6, a specific example of $\alpha_{\mathrm{m}}(v_{\mathrm{r}}, z)$ for a smooth transition between the elastic and plastic behaviour is

$$\alpha_{\mathrm{m}}(v_{\mathrm{r}}, z) = \frac{1}{2} \sin\left(\pi \frac{z - \frac{z_{\mathrm{ss}}(v_{\mathrm{r}}) + z_{\mathrm{ba}}}{2}}{z_{\mathrm{ss}}(v_{\mathrm{r}}) - z_{\mathrm{ba}}} \right) + \frac{1}{2}. \tag{27}$$

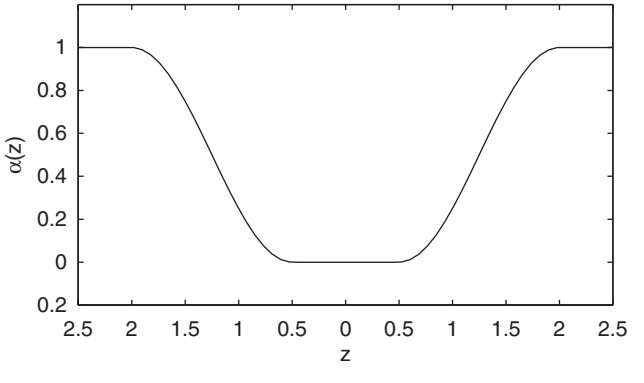

Figure 6. An example of the smooth elastic-to-plastic transition provided by $\alpha_{\mathrm{m}}(v, z)$ where $z_{\mathrm{ba}} = 0.5$ and $z_{\mathrm{ss}}(v_{\mathrm{r}}) = 2.0$.

4. Simulation using discrete elasto-plastic model

As mentioned in the introduction section of this paper, the emulation of friction force's dynamic characteristics at the road/tyre interface is important for developing EV control systems. The dynamic friction models need to be discretised for the digital controller to compute the generated torque of the dynamometer. The bilinear transformation can be applied to discretise the LuGre model

$$z_k = \frac{1 - \frac{T_s}{2}\frac{\sigma_0|v_{r,k-1}|}{g(v_{r,k-1})}}{1 + \frac{T_s}{2}\frac{\sigma_0|v_{r,k}|}{g(v_{r,k})}} z_{k-1} + \frac{T_s/2}{1 + \frac{T_s}{2}\frac{\sigma_0|v_{r,k}|}{g(v_{r,k})}}(v_{r,k} + v_{r,k-1}) \tag{28}$$

$$F_k = F_n\left[\left(\sigma_0 - \sigma_1\frac{\sigma_0|v_{r,k}|}{g(v_{r,k})}\right)z_k + (\sigma_1 + \sigma_2)v_{r,k}\right] \tag{29}$$

where T_s is the sampling time. Similarly the discrete elasto-plastic model is as in the following:

$$z_k = \frac{1 - \frac{T_s}{2}\alpha(z_{k-1}, v_{r,k-1})\frac{\sigma_0|v_{r,k-1}|}{g(v_{r,k-1})}}{1 + \frac{T_s}{2}\alpha(z_k, v_{r,k})\frac{\sigma_0|v_{r,k}|}{g(v_{r,k})}} z_{k-1} + \frac{T_s/2}{1 + \frac{T_s}{2}\alpha(z_k, v_{r,k})\frac{\sigma_0|v_{r,k}|}{g(v_{r,k})}}(v_{r,k} + v_{r,k-1}) \tag{30}$$

$$F_k = F_n\left[\left(\sigma_0 - \alpha(z_k, v_{r,k})\sigma_1\frac{\sigma_0|v_{r,k}|}{g(v_{r,k})}\right)z_k + (\sigma_1 + \sigma_2)v_{r,k}\right]. \tag{31}$$

However, the function $\alpha(z_k, v_{r,k})$ and z_k depend on each other. In order to avoid this interaction (i. e. algebraic loop), a simple solution is to adopt $\dot{z} \approx z_k - z_{k-1}/T$. But the one sample delay introduced by taking the back-forward difference is known to lead to inaccuracy and even instability in simulations. Therefore, in this paper an iterative Newton–Raphson technique is used to find a local zero (i.e. z_k) of the below function $f(x)$ using z_{k-1} as an initial guess:

$$f(x) = x - \frac{A}{1 + B \cdot \alpha(x, v_{r,k})}. \tag{32}$$

Observing Equation (30) gives

$$A = \left(1 - \frac{T}{2}\alpha(z_{k-1}, v_{r,k-1})\frac{\sigma_0|v_{r,k-1}|}{g(v_{r,k-1})}\right)z_{k-1} + \frac{T}{2}(v_{r,k} + v_{r,k-1}) \tag{33}$$

$$B = \frac{T}{2}\frac{\sigma_0|v_{r,k}|}{g(v_{r,k})}. \tag{34}$$

The derivative of $f(x)$ is

$$f'(x) = 1 + \frac{A}{[1 + B \cdot \alpha(x, v_{r,k})]^2} B \cdot \alpha'(x, v_{r,k}). \tag{35}$$

And the derivative of $\alpha(x, v_{r,k})$ is also a piecewise function:

$$\alpha'(x, v_{r,k}) = \begin{cases} 0, & \alpha(x, v_{r,k}) = 1 \text{ or } 0 \\ \frac{1}{2}\cos\left(\pi\frac{x - \frac{z_{ss}(v_r) + z_{ba}}{2}}{z_{ss}(v_r) - z_{ba}}\right)\frac{\pi}{z_{ss}(v_{r,k}) - z_{ba}}, & \text{else} \end{cases} \tag{36}$$

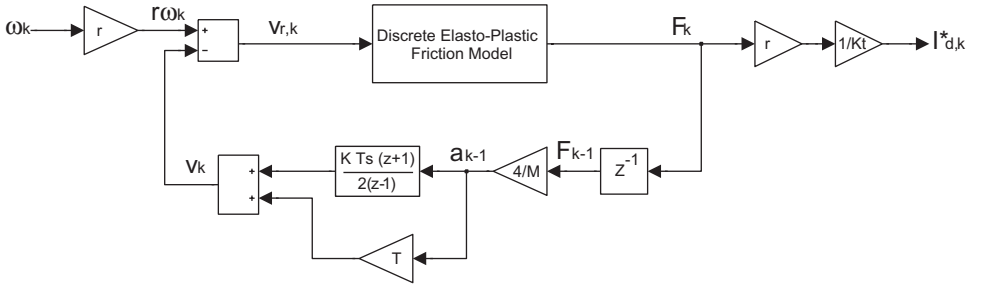

Figure 7. Block diagram of emulating dynamic friction using dynamomter.

Simulations show that five iterations of the Newton–Raphson method typically have a good convergence to the solution. After finding z_k, the friction force F_k is calculated using Equation (31). The block diagram of emulating the dynamic friction force using the dynamometer is shown in Figure 7.

Therefore the motor current command of the dynamomter is

$$i^*_{\mathrm{d},k} = \frac{F_k \cdot r}{K_\mathrm{t}} \tag{37}$$

where K_t is dynamometer's torque constant. Again vehicle velocity v_k is dependent on F_k. Here v_k is simply approximated by the first-order Taylor series expansion using F_{k-1}:

$$a_{k-1} = \frac{F_{k-1}}{M/4} \tag{38}$$

$$v_k \approx v_{k-1} + a_{k-1}T = \frac{T}{2}\frac{1+z^{-1}}{1-z^{-1}}a_{k-1} + a_{k-1}T \tag{39}$$

where v_{k-1} is calculated by the trapezoidal integration of the acceleration $\{a_1, \ldots, a_{k-1}\}$.

5. A case study: DOB-based anti-skid control

In this paper, a simple DOB-based anti-skid control strategy is introduced to test the emulation using the dynamic elasto-plastic road/tyre friction model [12]. In complete road/tyre adhesion, the dynamics of a quarter vehicle can be modelled as

$$T_\mathrm{m} = \left(J_\mathrm{w} + \frac{M}{4}r^2\right)\dot{\omega}. \tag{40}$$

Here $J_n \doteq J_\mathrm{w} + (M/4)r^2$ is defined as the nominal inertia for the above ideal road/tyre interaction. The skid of one wheel on a low μ road surface can be considered to be a sudden decrease of vehicle's equivalent inertia J_v from its nominal value, $(M/4)r^2$. In the extreme case when road/tyre friction force disappears, J_v becomes zero which will lead to a complete wheel skid. Therefore, the over acceleration of the wheel will be prevented if the equivalent inertia J_v felt by the drive motor is kept as same as its nominal value under any road condition. This can be achieved by introducing a DOB-based anti-skid controller.

As shown in Figure 8(a), using the inverse dynamic model of $J_n s$, the necessary drive torque $\hat{T}_\mathrm{m}$ can be estimated that generates the same virtual angular acceleration of a body with

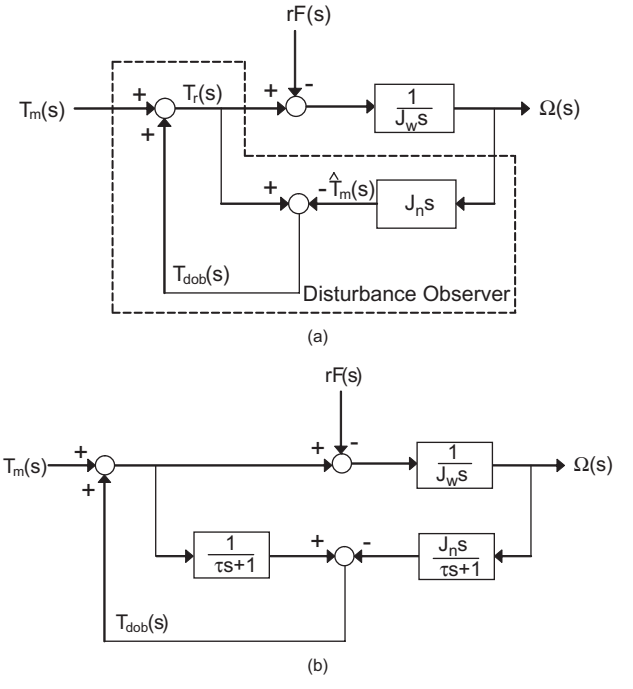

Figure 8. DOB-based anti-skid controller. (a) Ideal DOB; (b) DOB with Q-filter.

nominal inertia J_n as the wheel's real acceleration. With the configuration of the DOB shown in Figure 8(a), the relationship among T_{m}, T_{dob}, T_{r} and ω as follows:

$$T_{\mathrm{r}}(s) = T_{\mathrm{m}}(s) + T_{\mathrm{dob}}(s) \tag{41}$$

$$T_{\mathrm{dob}}(s) = T_{\mathrm{r}}(s) - J_n s\Omega(s) \tag{42}$$

$$J_{\mathrm{w}} s\Omega(s) = T_{\mathrm{m}}(s) + T_{\mathrm{dob}}(s) - rF(s) \tag{43}$$

where T_{dob} is the output torque command calculated by the DOB. Consequently the dynamic of $1/J_w s$ will be cancelled and the transfer function relating to T_{m} and ω is always being $1/J_n s$, as shown in Equations (41) and (42). Namely whatever the road condition is, the equivalent inertia felt by the drive motor keeps constant as its nominal value J_n.

When the vehicle enters a slippery road, the sudden decrease of the road/tyre friction force will lead to rapid increase of the total torque being exerted on the wheel (Equation (13)). The fast acceleration of the wheel on the slippery road will easily cause the vehicle to skid. On the contrary, with the DOB-based anti-skid controller, the decrease of the friction force can be automatically compensated by the output torque command T_{dob} of DOB, which is in the opposite direction of T_{m} because in such a case $\hat{T}_{\mathrm{m}}$ is always larger than T_{r} (Figure 8(a)).

However, the inverse dynamic should be avoided in practice. As shown in Figure 8(b), a lowpass filter called Q-filter can be introduced to avoid the direct computation of the inverse dynamic model $J_n s$. The Q-filter restricts the effective bandwidth of the DOB. A well-designed Q-filter provides good trade-off between the disturbance estimation performance versus the stability robustness and noise sensitivity [13]. In this paper, the DOB is also discretised using the bilinear transformation.

6. Experimental results

Emulation of the road/tyre longitudinal interaction is carried out based on the proposed discrete elasto-plastic dynamic friction model. The test bench is a torsional system as shown in Figure 9. In the torsional system, the flywheels of drive side and load side are connected with a long torsional shaft; while the drive torque is transmitted from the drive servomotor to the shaft by gears with gear ratio 1:2. In the experiment, the load servomotor is used as the dynamometer. The maximum output torque of the two brushless DC servomotors is ± 3.84 Nm. The angular position and speed of the two motors are detected by optical encoders with a resolution of 8000 pulses per revolution.

In order to minimise the flexibility of the test bench, a thick shaft is selected to connect the drive and load sides. The diameter of the shaft is 20 mm and its elastic coefficient is 1.5315×10^3 Nm/rad. Two flywheels are attached to each servomotor. The total inertia J_t including the inertia of drive motor, the dynamometer and connecting shaft is $6.9360 \times 10^{-3}\,\mathrm{kg \cdot m^2}$. For the sake of simplicity, the wheel inertia J_w is taken as same as J_t for the experiment. Considering the limitation of motors' maximum output torque, a small quarter-vehicle mass is selected such that the normal force F_n equals $15\,\mathrm{kg\,m/s^2}$. And the wheel radius r is 0.25 m.

Data used for simulating the dynamic friction model are shown in Table 1, which is from the experimental data [11,14]. The configuration of the dynamic emulation of the tyre/road longitudinal interaction with the DOB-based anti-skid controller is shown in Figure 10. The DOB-based anti-skid control is used as a case study for developing EV control systems using the dynamic emulation. In Figure 10, $T_{m,ref}$ and $T_{d,ref}$ are the reference commands for the output torque of the drive motor and the dynamometer, respectively. V is the vehicle's linear speed.

Experiments are carried out with constant torque command of $T_{m,ref}$ for the drive motor after 0.5 s as an input accelerating torque. The constant $T_{m,ref}$ is determined by having a vehicle

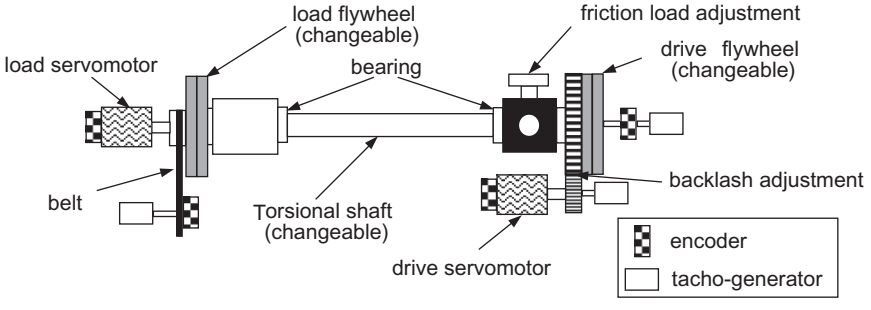

Figure 9. Experimental setup of the test bench.

Table 1. Data used for dynamic friction model simulation.

Parameter	Value
σ_0	$316\,\mathrm{m^{-1}}$
σ_1	1.0 s/m
σ_2	0.0005 s/m
μ_c	0.69
μ_s	1.779
v_s	3.5 m/s
z_{ba}	0.7

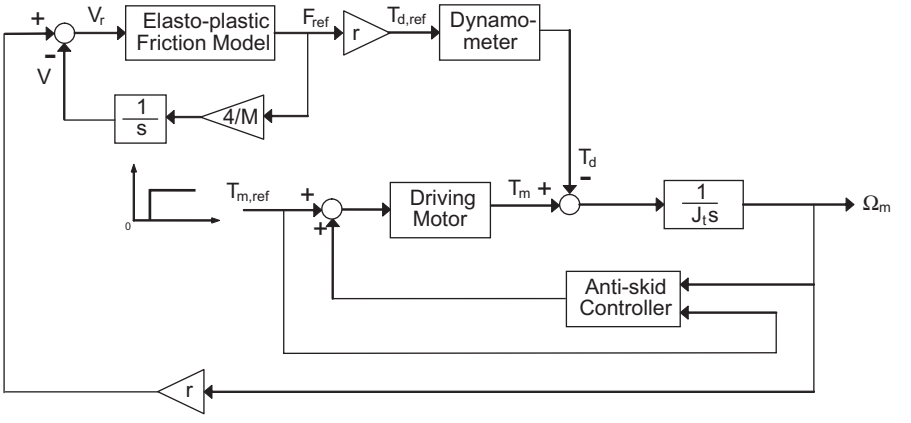

Figure 10. Configuration of the dynamic tyre/road friction emulation.

acceleration $\mathrm{d}V/\mathrm{d}t = 10\,\mathrm{m/s^2}$ under ideal complete road/tyre adhesion, i.e.

$$T_{\mathrm{m,ref}} = \frac{10}{r}\left(J_{\mathrm{w}} + \frac{M}{4}r^2\right). \tag{44}$$

A good road/tyre adhesion ($\theta = 1.0$) is assumed at the beginning of the emulation. From 2.0 s, θ is changed to 0.1, which emulates the dynamic behaviour of a vehicle suddenly entering a slippery road condition. The noises contained at the beginning of the time response of the slip rate is caused by the encoder's quantisation noise (see Figure 11(b)). Reducing the encode quantisation noise is important for further improving the emulation's accuracy. The discussion on overcoming this noise is beyond the scope of this paper.

As shown in Figure 11, without the anti-skid control, severe wheel skid occurs at 2 s when tyre/road adhesion level θ suddenly decreases to 0.1. Due to the sudden decrease of road/tyre friction force, the total torque being exerted on the wheel will rapidly increase, which could cause the wheel to skid. During the wheel skid, the side force generated by the wheel will also be dramatically decreased. This could lead to unstable vehicle lateral motion, such as dangerous spin motion.

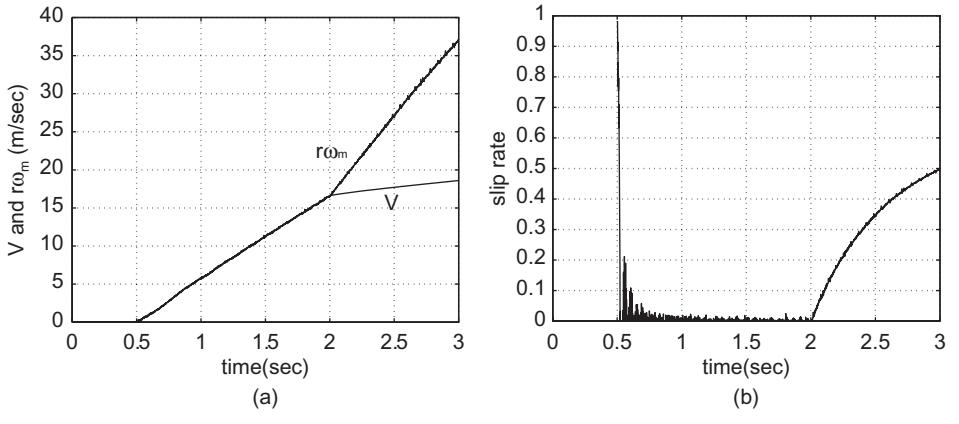

Figure 11. Emulation results without DOB-based anti-skid control. (a) V and $r\omega_{\mathrm{m}}$; (b) slip rate.

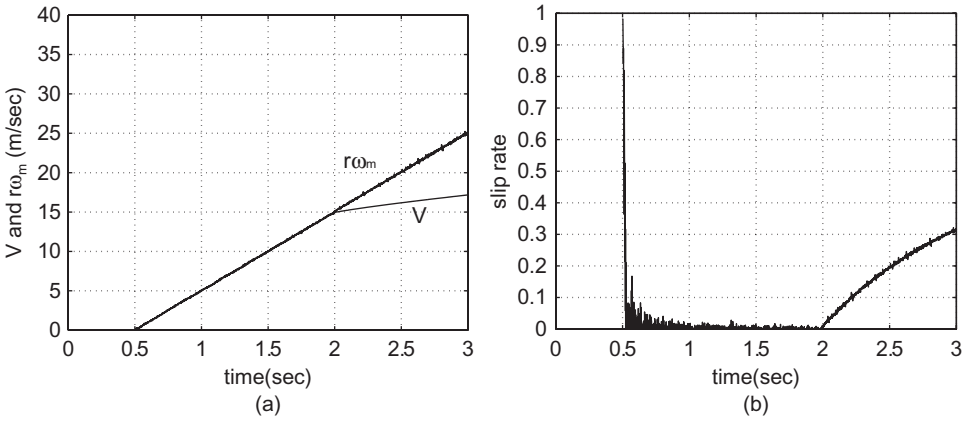

Figure 12. Emulation results with DOB-based anti-skid control. (a) V and $r\omega_{\mathrm{m}}$; (b) slip rate.

With DOB-based anti-skid control, the rapid increase of the slip rate is effectively suppressed as shown in Figure 12(b). The sudden decrease of the road/tyre friction force is automatically compensated by adding T_{m} with the output torque of the DOB, which is in the opposite direction. It is interesting to notice that the time response of the wheel speed V_{w} keeps having a same slope even with the sudden variation of θ, as shown in Figure 12(a). And the equivalent linear acceleration of the wheel is exactly 10 m/s^2, which is the same value of the acceleration with an ideal complete road/tyre adhesion. This observation verifies the basic consideration of the DOB-based anti-skid control, i.e. keeping constant equivalent inertia felt by the vehicle's drive motor under any road condition.

Another advantage of the dynamic emulation approach proposed in this paper is the ease of emulating various vehicle masses M. As shown in the block diagram of Figure 10 and the corresponding experimental results in Figure 13, by simply adjusting the parameter M or F_n, the transient behaviours of the vehicle and the drive motor can be emulated under a different vehicle mass. The method of using the inverse model or introducing the complicated model speed tracking approach mentioned in Section 2 to avoid the computation of the inverse dynamics is not needed.

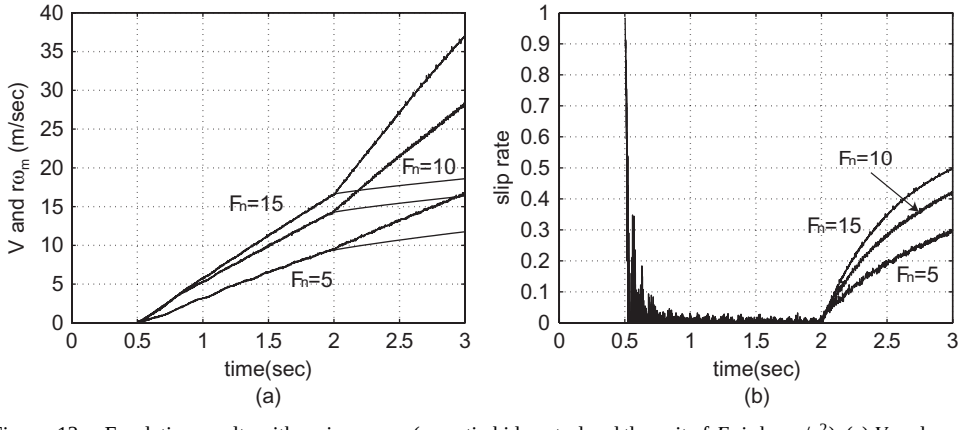

Figure 13. Emulation results with various mass (no anti-skid control and the unit of F_n is kg m/s^2). (a) V and $r\omega_{\mathrm{m}}$; (b) slip rate.

7. Summary

In this paper, a systematic approach on dynamic emulation of the road/tyre longitudinal interaction is proposed for developing EV control systems. Compared with the static friction models, dynamic friction models are more adequate for capturing the transient behaviour during braking and acceleration, which is important for validating the design of EV control systems in laboratory facilities. The proposed dynamic model is an elasto-plastic model based on the well-known LuGre model, but corrects LuGre model's spurious unbounded drift problem. For the digital implementation of the model using bilinear discretisation, the Newton–Raphson method is introduced to solve the algebraic loop problem. A DOB-based anti-skid controller is used as a case study to test the proposed dynamic emulation. Experimental results show the dynamic emulation is able to capture the transient behaviour of the road/tyre friction force and validate the effectiveness of the anti-skid controller. It is expected that this dynamic emulation approach will be useful for developing high-performance EV control systems such as more effective ABS and TCS systems. At the same time, the friction model used in this paper is a lumped friction model assuming a point road/tyre friction contact. A more realistic assumption is that a contact patch exists between the road and the tyre with associated normal force distribution. The discussion on introducing the distributed friction model, its necessity and comparison with the lumped friction model for the dynamic road/tyre friction emulation may be included in future works.

References

[1] Y. Hori, *Future vehicle driven by electricity and control-research on four-wheel-motored 'UOT Electric March II'*, IEEE Trans. Ind. Electron. 51(5) (2004), pp. 954–962.

[2] R.M. Schupbach and J.C. Balda, *A versatile laboratory test bench for developing powertrains of electric vehicles*, Proceedings of Vehicular Technology Conference 2002-Fall, Vancouver, Canada, Vol. 3, 2002, pp. 1666–1670.

[3] S.C. Oh, *Evaluation of motor characteristics for hybrid electric vehicles using the hardware-in-the-loop concept*, IEEE Trans. Veh. Technol. 54(3) (2005), pp. 817–824.

[4] G. He, F. Sun, and J. Xing, *Dynamic simulation and experiment of electric drive system on test bench*, Proceedings of IEEE International Conference on Vehicular Electronics and Safety 2007, Beijing, China, 2007.

[5] I. Alcalá, A. Claudio, and G. Guerrero, *Test bench to emulate an electric vehicle through equivalent inertia and machine DC*, Proceedings of Power Electronics Congress 2008, Cuernavaca, Morelos, Mexico, 2008, pp. 198–203.

[6] Z.H. Akpolat, G.M. Asher, and J.C. Clare, *Dynamic emulation of mechanical loads using a vector controlled induction motor-generator set*, IEEE Trans. Ind. Electron. 46(2) (1999), pp. 370–379.

[7] M. Short, M.J. Port, and Q. Huang, *Simulation of vehicle longitudinal dynamics*, Tech. Rep. ESL 04/01, Embedded Systems Laboratory, University of Leicester, UK, 2004.

[8] C. Canudas de Wit, P. Tsiotras, E. Velenis, M. Basset, and G. Gissinger, *Dynamic friction models for road/tire longitudinal interaction*, Veh. Syst. Dyn. 39(3) (2003), pp. 189–226.

[9] H. Olsson, K.J. Åström, C. Canudas de Wit, M. Gäfvert, and P. Lischinsky, *Friction models and friction compensation*, Eur. J. Control 4(3) (1998), pp. 176–195.

[10] C. Canudas de Wit, H. Olsson, K.J. Åström, and P. Lischinsky, *A new model for control of systems with friction*, IEEE Trans. Autom. Control 40(3) (1995), pp. 419–425.

[11] P. Dupont, V. Hayward, B. Armstrong, and F. Altpeter, *Single state elastoplastic friction models*, IEEE Trans. Autom. Control 47(5) (2002), pp. 787–792.

[12] H. Fujimoto, T. Saito, T. Akio, and T. Noguchi, *Motion control and road condition estimation of electric vehicles with two in-wheel motors*, Proceedings of the 2004 IEEE Intemational Conference on Control Applications, Taipei, Taiwan, 2004, pp. 1266–1271.

[13] C.J. Kempf and S. Kobayashi, *Disturbance observer and feedforward design for a high-speed direct-drive positioning table*, IEEE Trans. Control Syst. Technol. 7(5) (1999), pp. 513–526.

[14] K. Deng, K. Li, L. He, and Q. Xia, *Dynamic tire model for vehicle emergency braking simulation* (in Chinese), Trans. Chin. Soc. Agric. Machinery 38(12) (2007), pp. 11–15.